JCI The Journal of Clinical Investigation

# DNA-PK inhibition enhances neoantigen diversity and increases T cell responses to immunoresistant tumors

Allison Joy Nielsen, … , Breelyn Ann Wilky, Eduardo Davila

*J Clin Invest.* 2024. https://doi.org/10.1172/JCI180278.

Research In-Press Preview Immunology Oncology

## Graphical abstract

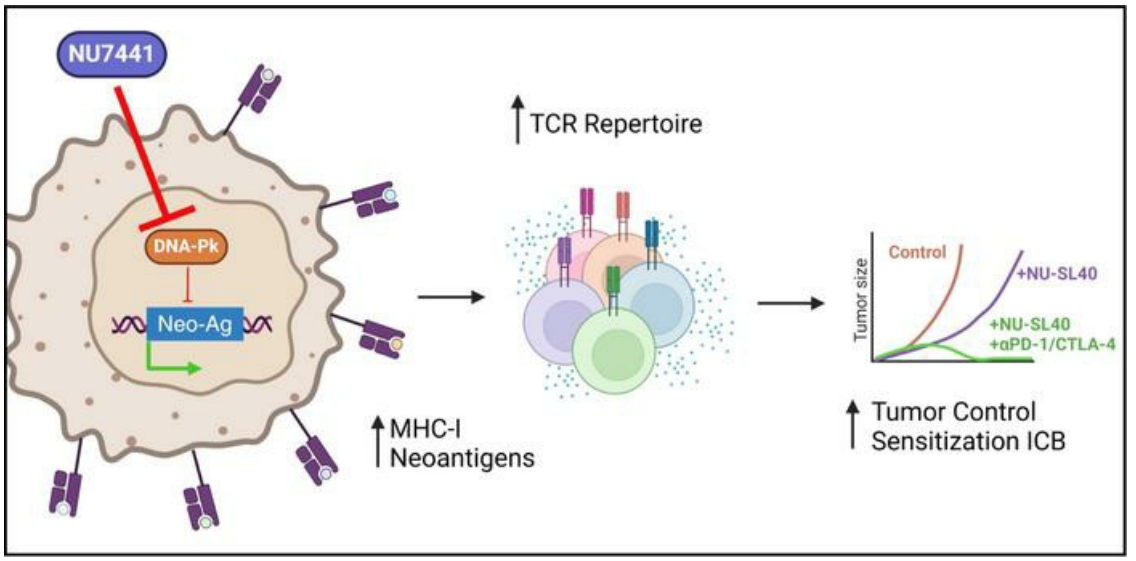

# DNA-PK inhibition enhances neoantigen diversity and increases T cell responses to immunoresistant tumors

Allison Joy Nielsen[1]*, Gabriella Kyra Albert[1]*, Amelia Sanchez[1], Jiangli Chen[1,2], Jing Liu[1], Andres Sebastian Davalos[1], Degui Geng[1,2], Xander Bradeen[1], Jennifer D. Hintzsche[3], William Robinson[1,2,4], Martin McCarter[1,4,5], Carol Amato[1], Richard Tobin[1,5], Kasey Couts[1,4], Breelyn Ann Wilky[1,4], Eduardo Davila[1,2,4]

[1] Department of Medicine, Division of Medical Oncology, University of Colorado School of Medicine, Aurora, CO, 80045, USA. [2] Department of Veterans Affairs, Research Service, Rocky Mountain Regional Veterans Affairs, Aurora, CO, USA. [3] PherDal Science, Dixon, IL, 61021, USA. [4] University of Colorado Comprehensive Cancer Center, University of Colorado School of Medicine, Aurora, CO, 80045, USA. [5] Department of Surgery, University of Colorado School of Medicine, Aurora, CO, 80045, USA.

**Conflict-of-interests.** E. Davila declares research support from and receives consulting fees from TrAMPoline Pharma Inc., outside the submitted work. M. McCarter declare research support from Merck, Taiho and NCCN not related to this work. All other authors declare no potential conflicts of interest.

**Corresponding author:** Eduardo Davila, 12801 E. 17th Ave, Aurora, CO, 80045. 303-848-0300. Eduardo.Davila@cuanschutz.edu

**Abstract**

Effective antitumor T cell activity relies on the expression and MHC presentation of tumor neoantigens. Tumor cells can evade T cell detection by silencing the transcription of antigens or by altering MHC machinery resulting in inadequate neoantigen-specific T cell activation. We identified DNA-PK inhibitor (DNA-PKi) NU7441 as a promising immunomodulator that reduced immunosuppressive proteins while increasing MHC-I expression in a panel of human melanoma cell lines. In tumor-bearing mice, combination therapy using NU7441 and immune adjuvants STING ligand and CD40 agonist (NU-SL40) substantially increased and diversified the neoantigen landscape, antigen presenting machinery, and consequently substantially increased both the number and repertoire of neoantigen-reactive tumor infiltrating lymphocytes (TILs). DNA-PK-inhibition or knockout promoted transcription and protein expression of various neoantigens in human and mouse melanomas and induced sensitivity to ICB in resistant tumors. In patients, *PRKDC* levels inversely correlated with MHC I expression and CD8 TILs but positively correlated with increased neoantigen loads and improved responses to ICB. These studies suggest that inhibiting DNA-PK activity can restore tumor immunogenicity by increasing neoantigen expression and presentation and broadening the neoantigen-reactive T cell population.

## Introduction

T cell-based cancer immunotherapies exploit the T-cell's ability to selectively recognize and destroy cancer cells while sparing non-cancerous cells, representing one of the most effective cancer treatments available for different malignancies including melanoma. Recent examples include antibody blockade of checkpoint receptors (e.g., cytotoxic T-lymphocyte antigen-4 (CTLA-4), programmed death-1 (PD-1) or its ligand (PD-L1), adoptive cell transfer (ACT), tumor-infiltrating lymphocytes (TIL), or T cells engineered to express tumor-reactive T cell receptors (TCR) (4, 7). The advances achieved through these treatments have sparked the development of newer therapies that enhance the activation of anti-tumor T cell responses as well as investigation into the mechanisms underlying why most patients do not benefit from single agent immunotherapies.

Uncontrolled tumor growth in patients characterizes the immune system's failure to recognize and/or destroy tumor cells. Often, weak tumor immunogenicity hinders the immune system's ability to control tumor growth and arises from low surface expression of major histocompatibility complex (MHC) I and II, limited expression of antigenic epitopes, or expression of antigens with low affinities for MHC. Importantly, T cells with high affinity toward self-tumor-associated antigens (TAA) are deleted in the thymus resulting in a repertoire of circulating T cells with limited anti-tumor activity. These conditions create an inadequate immune response that facilitates cancer cell growth and mechanisms of tumor immune evasion.

Immune recognition of neoantigens is a key mechanism of the potent anti-cancer responses observed in patients receiving checkpoint blockade and ACT of TILs (1-3). Neoantigens arise from non-synonymous somatic DNA mutations that change amino acid protein sequences. These mutated peptides are processed and loaded onto MHC I or II, presented on the cancer cell surface, and subsequently recognized by cytotoxic T cells (4, 5). Clinical data suggests that treatment with anti-CTLA-4 and anti-PD-1 antibodies alters and diversifies the TCR repertoire within the tumor microenvironment and is positively associated with anti-tumor responses (1-3).

For example, studies of lung cancer and melanoma patients undergoing checkpoint blockade therapy indicate that tumors from responding patients expressed elevated numbers of somatic mutations (6, 7). These studies also reveal that neoantigen expression is heterogenous even within the same tumor sample; some neoantigens are clonally present in most cancer cells within the same patient, while other neoantigens are sub-clonal and expressed in a fraction of cancer cells (8). Thus, strategies targeting neoantigens are tumor specific. Although reports have highlighted that changes in the TCR repertoire can indicate anti-tumor activity, they have yet to elucidate how the functional capacity (cytokine production, effector function, phenotypic distinctions) associated with TCR repertoire changes correlates with anti-tumor immunity.

We previously screened a library of ~2,500 clinically relevant compounds and evaluated their ability to enhance the immunogenicity of melanoma (9) and improve dendritic cell (DC) function (10). Of these drugs, we identified several DNA-protein kinase (DNA-PK) inhibitors that enhanced MHC I expression levels, sensitized melanoma cells to T cell-mediated killing in vitro and enhanced the ability of DCs to activate tumor-reactive T cells including NU7441, NU7026, and KU-0060648. Of these, NU7441 was identified as the most effective. DNA-PK is a serine/threonine protein kinase composed of a Ku heterodimer (Ku70 & Ku80) and a catalytic subunit (DNA-PKcs) that has a central role in the DNA damage response and maintenance of genomic stability (11). In this role, DNA-PK mediates ligation of DNA double-strand breaks through nonhomologous end joining (12). At present, several therapeutic compounds are in clinical testing assessing the anti-tumor efficacy of targeting DNA-PK kinase activity [NCT02516813, NCT02316197, NCT01353625, and NCT02833883]. Previously, the proposed mechanisms of action were founded on the idea that DNA-PK inhibition will control tumor growth by altering DNA repair. Further, several groups reported that tumor antigen expression can be upregulated by inhibiting key signaling pathways overly activated in melanoma (9, 13-15). Notably, we present evidence that DNA-PK inhibition has potent immunostimulatory effects on melanoma cells demonstrated through investigation of the mechanistic underpinnings of DNA-

PK inhibition on TIL infiltration, tumor antigen expression, and TCRvβ diversity and functional capacity.

Herein, we examined the combinatorial effects of treatment with NU7441 plus immune stimulation with interferon-α inducer STING agonist (STGL) and CD40 agonist in murine melanoma models on the infiltration of tumor-reactive effector CD8+ TIL and skewing of the tumor-reactive TCRvβ repertoire. We also revealed associations between changes in the TCRvβ repertoire and the diversification of neoantigen expression profiles in murine melanoma models and melanoma patients. In melanoma patients treated with anti-PD-1 and anti-CTLA-4, DNA-PK transcript (*PRKDC)* levels inversely correlated with CD8 and MHC I transcripts while mutations in DNA-PK correlated with increased tumor mutation burden and neoantigen load. Furthermore, while combination anti-PD-1 and anti-CTLA-4 blockade was ineffective against weakly immunogenic melanoma tumors in mice, adding DNA-PKi (NU7441) in conjunction with STGL and anti-CD40 (NU-SL40) or knocking out DNA-PK in tumors resulted in tumor regression in 75%-100% in mice. Our results suggest that DNA-PK inhibition combined with immune adjuvants enhances tumor immunogenicity by increasing neoantigen expression and presentation resulting in a broader panel of neoantigen reactive T cells with heightened functional capacity in mice and melanoma patients. This study highlights an especially relevant and promising second line therapy for individuals with tumors bearing low neoantigen loads.

## Results

***Combination DNA-PK inhibition plus immune adjuvants drive melanoma regression via a CD8 T cell-dependent mechanism.*** We previously identified the DNA-PKi NU7441 as a potent drug that decreased expression of numerous immunomodulatory proteins, including CD55, CD73, CD155, PD-L1 and NGFR and increased HLA class I expression in vitro (9). Here, we investigated the anti-melanoma activity of combination therapy using NU7441 (NU) and immune adjuvants STING ligand (SL) plus CD40 antibody agonist (NU-SL40) in mice bearing immunoresistant B16-F10 melanoma tumors. Female C57BL/6 mice with established tumors received treatment with either DNA-PKi (NU), STING ligand plus anti-CD40 (SL40), or combination treatments NU-SL40 or SL40-NU; treatment regimen in **Figure 1A**. The individual treatments of DNA-PKi and SL40 alone as well as SL40-NU combination did not mediate substantial tumor control, exhibiting tumor growth comparable to untreated mice, **Figure 1B**. In sharp contrast, NU-SL40 mediated tumor regression with sustained anti-tumor immunity and prolonged mouse survival for 40 days, **Figure 1C**. As the NU-SL40 combination treatment regimen is intended to activate tumor-reactive T cells, we validated the role of CD8 T cells. We observed that CD8 T cell depletion ablated the anti-tumor activity of NU-SL40 therapy, and reduced survival to the same as untreated mice, **Figure 1B and 1C**. Notably, B16-F10 tumors have been shown to promote cachexia characterized by weight loss, skeletal muscle wasting, and adipose tissue loss, which can be further exacerbated by immunostimulatory agents such as STING agonists and checkpoint blockade (16). Despite potent anti-tumor immune responses, mouse weights remained similar between treatment groups, **Supplemental Figure S1A**.

Altogether, these data indicate that neither DNA-PKi nor immune adjuvants alone generate productive antitumor responses. However, when combined in a specific order, NU-SL40 treatment generated effective tumor control dependent upon the activation of tumor-reactive CD8 T cells and without promoting cachexia.

***DNA-PK inhibition plus immune adjuvants induces clinically relevant gene signatures within the tumor microenvironment including enhanced signaling in inflammatory and antigen presenting pathways.*** Several profiling studies in clinical samples from cancer patients treated with checkpoint blockade have revealed distinct gene signatures associated with response to therapy, supporting their role in diagnosis and treatment of cancer (17-19). To understand the mechanistic underpinnings that generate potent anti-melanoma immune responses, we profiled changes to RNA in tumors from untreated mice, those treated with immune adjuvants alone, or in combination with DNA-PKi using the PanCancer Immuno Oncology (IO) NanoString assay. Compared to untreated mice, treatment with DNA-PKi or SL40 differentially regulated the expression of 7 RNA transcripts out of the 770 genes, **Figure 1D, left and middle panel**. In contrast, tumors from NU-SL40 treated mice upregulated 87 and downregulated 12 genes, **Figure 1D, right panel**. Genes differentially regulated within and between treatment groups are shown in **Supplemental Table S1**.

Pathway analysis of RNAs from NU-SL40-treated mice identified gene signatures associated with interferon signaling (26 RNAs), antigen presentation (21 RNAs), lymphoid and myeloid compartments (9 and 13 RNAs), cytotoxicity (13 RNAs) and cytokine and chemokine signaling (13 RNAs), among other genes outside these pathways relevant to inflammation anti-cancer pathways. **Figure 1E** shows a visual representation of the average transcript counts, fold-changes, and p-values in NU-SL40-treated tumors relative to untreated tumors. The greatest level of clustering was genes associated with antigen presentation and interferon signaling. β2m, a key structural protein of the MHC-I molecule, had the largest RNA count in NU-SL40 tumors indicating substantial upregulation of MHC-I. These data uphold our previous reports demonstrating that DNA-PKi increased MHC-I expression on melanoma and dendritic cells (9, 10). Additionally, several H2 genes associated with antigen presentation and interferon signaling were upregulated in NU-SL40 tumors (**Supplemental Table S1**). Specifically, *H2-Aa* and *H2-B1* participate in processing of exogenous peptides via MHC-II, and positively regulate

T cell differentiation and responses to interferon gamma (IFN-γ), respectively. *H2-K1* regulates endogenous peptide processing via MHC-I in a TAP-dependent manner, and positively regulates T cell cytotoxicity. In agreement with gene regulation favoring interferon signaling, guanylate binding protein (GBP) genes G*bp*2 and *Gbp3*, which are induced by IFNγ production and have been correlated with improved overall survival in cutaneous melanoma patients (20), were substantially upregulated in NU-SL40-treated mice. Increased expression of *Eif2ak2*, *Gbp3*, *Oas1*, *Ifit1*, *Ifit2*, *Ifit3*, *Psmb8* – genes associated with interferon signaling and cytotoxicity – were also observed with NU-SL40 treatment, and high expression of these genes is prognostic in melanoma (21). *Cxcl9*, an anti-tumor-associated chemokine that facilitates recruitment of TILs to the tumor, and *Ccl5*, an inflammatory chemokine that reflects levels of leukocyte infiltration (22), increased 22- and 16-fold in expression, respectively, following NU-SL40 treatment. *Nos2*, a gene indicative of reactive oxygen species production and typically a poor prognostic factor in melanoma (23), was the only common gene upregulated in NU-SL40, SL40 and NU treatments. NU-SL40 treatment downregulated 11 transcripts including tumor drivers *Myc*, *Tgfb2*, *Tlr4*, *Cd276*, and *Sox11*, and genes associated with melanoma metastasis including *ITGA4*, which facilitates tumor cell migration (24-26), **Figure 1F**. NU-SL40 also downregulated thymidylate synthase, *Tyms*, a critical enzyme in cell cycle progression, which is expressed at higher levels in metastatic melanoma (27).

We further evaluated changes in tumor-derived RNA associated with T cell activation. Granzyme A (*Gzma*), *Nkg7,* and CD3 subunit expression in NU-SL40-treated tumors were amongst the most upregulated genes relative to control groups, **Supplemental Figure S1B**. Lower expression of Granzyme A in melanoma patients treated with checkpoint inhibitors predicted unfavorable prognosis while high expression was correlated with CD8 T cell infiltration (28). Recently, NKG7 expression in TIL has been associated with cytotoxicity in melanoma and is upregulated in tumor antigen-specific CD8 TIL (29).

Collectively, these data indicate that treatment with DNA-PKi plus immune adjuvants (NU-SL40) mediates RNA profiles favoring tumor antigen processing and presentation, T cell activation, and chemokine production that promote T cell recruitment.

***DNA-PK inhibitor in combination with immune adjuvants but not alone increases the number of activated tumor-infiltrating CD8 T cells.*** To validate the RNA expression profiles suggesting an increased number of activated TILs and to further investigate changes in immune cell distribution, we quantified and phenotypically characterized tumor immune cell infiltrates, **Figure 2A**. NU-SL40 combination treatment substantially increased the number of CD8+ TILs five-fold compared to individually treated or untreated groups. NU-SL40 treatment trended towards increasing NK cell numbers, however, these changes were not statistically significant. NU-SL40 also markedly reduced the number of B cell tumor infiltrates to nearly undetectable levels, **Figure 2A and Supplemental Figure S2.** Based on the reduction of B cells in tumors in response to combination treatment with NU-SL40, we investigated how this treatment regimen altered B cell numbers in the spleen and bone marrow. We observed that while NU-SL40 reduced B cell numbers in tumors it increased numbers in the spleen. In bone marrow, NU-SL40 did not impact the numbers of single positive CD19+ or CD20+ cells but increased the number of CD19+CD20+ cells in male mice, **Supplemental Figure S2**. The role that B cells play in melanoma immunity is not entirely clear as distinct B cell subsets with contrasting functions exist, such as activating and regulatory B cells, and the presence of B cells that promote the development of tertiary lymphoid structures. However, considering the anti-tumor effects mediated by NU-SL40, B cells could have played a regulatory role and their reduction in number contributed to enhanced anti-tumor CD8 T cell activity.

Surface expression of PD-1 and 4-1BB signifies cellular activation and expression on T cells has been shown to distinguish tumor-reactive T cells (30, 31). We found the majority of CD8 TIL collected from untreated mice or those treated with SL40 or DNA-PKi were 4-1BB$^{-}$ PD-1$^{-}$,

**Figure 2B and 2C**. In contrast, 59% of CD8 TIL from NU-SL40-treated mice expressed either one or both 4-1BB and PD-1 markers and demonstrated a three-fold increase in total PD-1$^+$ and two-fold increase in 4-1BB$^+$ single positive populations when compared to untreated mice, **Figure 2B and 2C, right panels**. Further, the expression levels of these molecules on a per-cell-basis were elevated compared to control groups (**Figure 2B,** adjunct histograms). Our data also show that NU-SL40 treatment promoted the activation and infiltration or expansion of CD8 T cells to the tumor. NU-SL40 treatment induced skewing of T cell populations in favor of CD8 over CD4 TIL when compared to untreated, DNA-PKi- and SL40-treated mice, **Figure 2D**.

We next performed UMAP analysis of CD45+ lymphoid and myeloid populations to evaluate the distribution and relationship of infiltrating immune cells in response to treatment. The lymphoid distribution in NU-SL40 treatment confirmed increases in CD8 TIL, while also revealing a spatial relationship between CD8+ and NK1.1 cells, **Figure 2, top panel**. These data suggest that NU-SL40 treatment may give rise to an NKT cell population. Notably, B cells are nearly lost in NU-SL40–treated tumors. Myeloid and DC distribution, **Figure 2E, bottom panel,** reveals an overall decrease in myeloid-derived suppressor cells (MDSC) in NU-SL40-treated mice.

Altogether, these data demonstrate that combination treatment, but not individual treatments promote the infiltration of tumor-reactive CD8 T cells with a highly activated phenotype while reducing the frequency of T cell suppressive DCs and MDSCs.

***NU-SL40 skews the CD8 TIL TCRvβ diversity with increased recognition of tumor cells.*** Numerous studies have suggested that skewing of TCRvβ diversity in the blood and tumor following checkpoint blockade is associated with better outcomes and progression-free survival (32-34). We evaluated the CD8 TCRvβ repertoire by staining fifteen murine TCRvβ chains as depicted in **Figure 3A.** A representative staining of CD3+CD8+TCRvβ6+ TIL from untreated or NU-SL40-treated mice bearing B16-F10 tumors is shown in **Figure 3A, right panel**. **Figure 3B**

shows UMAP analysis of CD8 TIL clustered by TCRvβ group in each treatment and demonstrates considerably larger clusters in select TCRvβ families from NU-SL40-treated tumors indicating a substantial increase in CD8 TIL relative to control groups. **Figure 3C** illustrates changes in the distribution of CD8 TIL TCRvβ family members compared to untreated mice. In SL40-treated mice, statistically significant decreases (blue bars) in TCRvβ chains 5.1-5.2, 8.1-8.2, 9, and 14 were observed compared to the untreated group, **Figure 3C**. Both NU and NU-SL40 treated mice exhibited substantial increases (red bars) in TCRvβ 6, while NU-SL40 additionally increased the frequency of TCRvβ 11, 12, and 13 compared to untreated mice, **Figure 3C**. We further evaluated surface expression of TCRvβ and CD8 proteins on TIL and found that TIL from NU-SL40-treated tumors increased TCR (3- to 12-fold) and CD8 (3- to 14-fold) expression density when compared to TIL from untreated or NU-treated tumors, **Supplemental Figure S3**. Changes in the TCRvβ repertoire and numbers of clonally expanded circulating T cells have been shown to reflect TIL function (35). We observed that several CD8 TCRvβ family members increased in circulation following combination treatment compared to all other groups, **Supplemental Figure S4**. In contrast, there was a global decrease of all CD4 TCRvβ family members in the blood of SL40- and NU-SL40-treated mice, **Supplemental Figure S4**. However, in NU-SL40-treated mice total CD4 TIL numbers were maintained and comparable between groups, **Figure 2A**. In summary, NU-SL40 treatment increased the total number of CD8 TIL and altered the TCRvβ repertoire of infiltrating and circulating CD8 T cells. These data are clinically relevant as changes in TCRvβ diversity is a biomarker for favorable outcomes in some cancers (36).

We next investigated the functional capacity of each CD8 TIL TCRvβ family member to respond to antigenic stimulation ex vivo. CD4/CD8 TIL were enriched (>98% purity) from the tumors of untreated or NU-SL40-treated mice and cultured with or without IFNγ-stimulated B16-F10 cells, **Figure 3D**. We then assessed the frequency of PD-1$^{+}$ Granzyme B (GzmB) producing CD8 TIL and investigated TCRvβ usage by flow cytometry; a representative flow plot

is shown in **Figure 3E**. In **Figure 3F**, the heatmap represents the sum of PD-1$^{+}$GzmB-producing CD8 TIL by expression of TCRvβ families with and without B16-F10 ex vivo stimulation. In the absence of antigen stimulation, TIL from untreated mice had relatively small numbers of PD-1$^{+}$GzmB$^{+}$ TIL (193 per 200,000 cells). In contrast, NU-SL40 treatment induced a 5.3-fold increase of PD-1$^{+}$GzmB$^{+}$ TIL (1042 cells). Amongst the various CD8 TIL TCRvβ family members increased by NU-SL40 treatment without B16-F10 stimulation, we found the greatest increase in TCRvβ 5.1/5.2 (10-fold), TCRvβ 8.3 (14-fold), TCRvβ 10b (63-fold), and TCRvβ 11 (17-fold). In the absence of antigenic stimulation, TIL from NU-SL40-treated mice moderately increased (2-fold) the number of PD-1$^{+}$GzmB$^{+}$ TIL and primarily belonged to TCRvβ family 6, 10b and 11, though, most TIL from untreated mice did not produce Granzyme B, **Figure 3E and 3F**. In sharp contrast, co-culture of B16-F10 tumor cells with TIL from NU-SL40-treated mice increased the numbers of PD-1$^{+}$GzmB$^{+}$ cells expressing TCRvβ 2 (10-fold), TCRvβ 9 (67-fold), TCRvβ 11 (8-fold), and to a smaller degree TCRvβ 5.1/5.2 (2-fold) and TCRvβ 8.3 (5-fold) compared with stimulated TIL from control mice, **Figure 3F**.

Collectively, these data highlight the ability for DNA-PK inhibition to elicit the activation of a unique group of tumor-reactive CD8 T cells, increase the diversity of tumor-specific TCRvβ members, and enhance the production of cytotoxic molecules.

***DNA-PK inhibition regulates tumor associated antigen and neoantigen expression in mouse and human melanoma.*** While performing in vitro culture of B16-F10 cells treated with NU7441, we observed that treatment gradually darkened cells and supernatants, suggesting an increase in melanin synthesis **Figure 4A and 4B**. In humans and mice, numerous proteins involved in melanin synthesis contain immunogenic CD8 epitopes that serve as TAAs (37). To better understand the transcriptional changes induced by DNA-PK inhibition in melanoma, we conducted RNA sequencing (RNA-seq) in B16-F10 melanoma cells treated with a vehicle control (DSMO) or NU7441 to explore changes to the antigen landscape, as described

previously (38). We used the fragments per kilobase of exon model per million reads mapped (FPKM) to estimate gene expression from our RNA-seq data. In agreement with predicted increases in melanin synthesis following treatment with DNA-PKi, we detected increased expression of genes in the melanin synthesis pathway which also serve as TAAs including *Pmel* (6.8-fold), *Trp53* (5.6-fold), *Tyrp1* (5.1-fold), *Tyr* (4.9-fold), *Dct* (4.1-fold), and *Mlana* (6.9-fold), **Figure 4C**. Increased RNA transcript levels were associated with increased protein expression, **Figure 4D**.

Upregulated expression of numerous tumor antigens following NU7441 treatment suggests that DNA-PK inhibition could regulate transcriptional machinery in a manner that alters expression of other genes including those coding for neoantigens. We found 91 neoantigens shared between DMSO and NU7441-treated melanoma cells, while 26 unique neoantigens were induced by the DNA-PKi, **Figure 4E**. The mutated gene and associated changes in amino acid sequence are shown in **Figure 4F, left**. The FPKM levels of NU7441-induced neoantigens and their predicted binding affinity to MHC-I (H2-Kb or Db) were also evaluated **Figure 4F**, **right**. Consistent with the idea that DNA-PK inhibition modified transcriptional machinery leading to increased transcription, we observed that NU7441 increased the transcript levels of several other shared neoantigens (**Supplemental Figure S5A**).

To examine whether these effects extended to human melanomas, we investigated the ability of DNA-PKi to alter the expression of clinically relevant TAAs that are currently targets for vaccine development or TCR engineering platforms. A tumor cell line with matched TIL was generated from a patient with cutaneous melanoma and cultured in the presence of DMSO or NU7441, **Figure 4G**. DNA-PK inhibition increased the transcript and protein levels of numerous TAAs several-fold, **Figure 4H and 4I**. We also investigated the direct role of DNA-PKi on TIL activity in vitro and found that at lower concentrations, DNA-PKi had no impact on IFN$\gamma$ or Granzyme B but at higher concentrations, dampened T cell activity, **Supplemental Figure S5B**. Despite these in vitro findings, combination DNA-PKi-immunotherapy demonstrated robust anti-

tumor responses (0.125mg/mouse/injection). We then investigated the anti-tumor TIL activity against a DNA-PKi-treated melanoma cell line generated from the same tumor. As shown in **Figure 4J**, DNA-PKi alone did not induce melanoma cell death as measured with Annexin-V. Further, co-culture of vehicle control-treated melanoma with paired TIL resulted in only moderate killing. In sharp contrast, pre-treatment with NU7441 of human melanoma cells followed by co-culture with autologous-TIL substantially increased T cell cytotoxicity.

Altogether, these data indicate that DNA-PK inhibition alters the tumor transcriptional profile resulting in both the induction of a unique panel of neoantigens while simultaneously increasing the levels of various TAAs and neoantigens. The ability of DNA-PKi to increase and diversify the tumor antigen landscape was associated with enhanced tumor immunogenicity as demonstrated by improved activation and killing by tumor-reactive TIL.

***NU-SL40 treatment promotes the generation of functional neoantigen-reactive CD8 TIL.***

Considering that TIL from NU-SL40-treated tumors exhibited increased response following B16-F10 stimulation (**Figure 3**) and that DNA-PKi increased neoantigen expression (**Figure 4**), we characterized the ability for TIL to recognize a panel of NU7441-induced neoantigens described in **Figure 4**. $CD3^+$ TIL isolated from untreated and NU-SL40-treated tumors were activated using mouse dendritic cells engineered to express tandem-minigenes (TMG) coding for various neoantigens, as described previously (39), **Figure 5A**. Each TMG codes for ten neoantigens and each neoantigen contains 15 amino acids down and upstream of the mutations (39, 40). We observed that TIL isolated from NU-SL40-treated mice were sensitive to several TMG-expressing DCs and produced substantially higher quantities of IFN$\gamma$ as compared with TIL from untreated tumors, **Figure 5B**. Notably, the induction of IFN$\gamma$ from TMG-DC stimulated NU-SL40 TIL compared to untreated TIL was detected between two different experiments, and although the intensity of response varied, the overall trend remained consistent, **Figure 5C**. These changes in CD8 TIL effector responses to different neoantigens implies an evolving tumor

antigen landscape in which NU-SL40 is capable of differentially activating TIL with distinct TCRvβ expression profiles.

We next investigated the ability of specific CD8 TIL TCRvβ family members to become activated by neoantigens evaluated by IFNγ and GzmB production by flow cytometry. The heatmaps in **Figure 5D and 5E** summarize the number of TIL and specify the TCRvβ family members that produced IFNγ and GzmB in response to stimulation with different TMGs. The numbers above each column are the sum of cytokine-producing TIL per TCRvβ family member while the sum of cytokine-producing TIL responding to specific TMGs is indicated by row. We observed that TIL expressing TCRvβ 2, 3, and 8.1/8.2 demonstrated the greatest degree of response against a broad array of TMGs based on IFNγ production relative to a GFP-TMG control, **Figure 5D**. In contrast, we did not detect appreciable numbers of IFNγ–producing TCRvβ 4, 8.3, 9, 10b, or 11 TIL. Individually, each TMG prompted cytokine production by a limited number of TCRvβ family members, **Figure 5D**. For example, TMG4 did not induce cytokine production while TMG1 only provoked TCRvβ 3 TIL to produce IFNγ. However, TMG2, TMG9.1, TMG9.2, TMG10, and TMG11 elicited robust IFNγ production from numerous TCRvβ groups while TMG3, TMG7, and TMG9.2 activated TIL to a lesser extent.

We also evaluated the TMG-DCs ability to elicit GzmB production by TIL from NU-SL40-treated mice. The most responsive TCRvβ family members were TCRvβ 4 and TCRvβ 11, which accounted for 64% of responding TIL, followed by TCRvβ 6 and TCRvβ 2. TMGs 2, 3, and 10, stimulated 29% of GzmB-producing TIL, **Figure 5E**. Most TMGs promoted GzmB production by at least two TCRvβ family members with TMGs 2, 3 and 10 stimulating 38% of T cells. Notably, the TCRvβ family members that produced GzmB differed from those that produced IFNγ. Specifically, the greatest number of GzmB–producing TIL belonged to the TCRvβ 4 and 11 families whereas TCRvβ 2, 3, and 8.1/8.2 predominately produced IFNγ.

Together, these findings highlight DNA-PKi's ability to increase the number of functionally active TIL populations and promote a more versatile TCRvβ repertoire reactive

against a broader, diverse panel of neoantigens. These data also underscore the generation of a distinct subset of neoantigen-reactive TIL capable of exclusively producing IFNγ or GzmB against different neoantigens.

***Alterations in the DNA-PK gene expression and sequence in melanoma patients treated with checkpoint immunotherapy correlate with CD8 TIL infiltration, neoantigens loads, and responses to therapy.*** In melanoma, CD8 TIL infiltration has been positively associated with MHC-I expression levels, high tumor mutation burden and neoantigen loads (41), as well as response to checkpoint inhibitors. A recent report by Tan et al. demonstrated that mutations in *PRKDC* could serve as predictive biomarkers for positive outcomes with checkpoint blockade in gastric cancers (42). Thus, we reviewed publicly available exome sequencing data from melanoma patients undergoing CTLA-4 or PD-1 blockade therapy to investigate potential correlations between *PRKDC* levels and response to checkpoint therapy (2, 33, 34). To uncover associations between CD8 infiltrates and the expression of MHC-I (*HLA-A*) with *PRKDC* (DNA-PK) levels, we analyzed melanoma patient data from TCGA. Both increased *CD8a* and *HLA-A* expression negatively correlated with *PRKDC* expression, suggesting that decreased DNA-PK expression and activity may promote CD8 tumor infiltration, **Figure 6A**. We observed that patients who responded to immunotherapy trended towards higher *CD8a* expression with longer overall survival trending towards lower *PRKDC* expression, **Figure 6B and 6C**.

The *PRKDC* gene encoding DNA-PKcs is a critical component of the DNA damage repair (DDR) pathway and mutations in the tumor DDR pathway can serve as important biomarkers for response to checkpoint-based immunotherapies. To further understand how alterations in the *PRKDC* gene correlated with response to immune checkpoint inhibition, we analyzed data from three melanoma clinical trials utilizing PD-1/CTLA-4 therapy (2, 33, 34) and found that a higher percentage of patients with altered (mutations, deletions, amplifications) *PRKDC* demonstrated

superior responses to immune checkpoint inhibition, **Figure 6D**. We further analyzed the exome sequencing data set for Tumor Mutation Burden (TMB) and Neoantigen Load and categorized patients for *PRKDC* expression as either normal (WT) or altered. We found that patients with *PRKDC* alterations had higher TMB and neoantigen load, **Figure 6E**. The increased TMB and neoantigen load in melanoma patients with *PRKDC* mutations or deletions supports our findings that DNA-PKi not only increases the expression of neoantigen transcripts but also induces what we considered to be a new panel of neoantigens.

As phosphorylation regulates the activity DNA-PKcs, we utilized immunohistochemistry to investigate the total and phosphorylated levels of DNA-PKcs in melanoma patients undergoing checkpoint blockade therapy and their response to treatment. The data in **Figure 6F** shows a mucosal-vulvovaginal melanoma sample with elevated levels of total and DNA-PK phosphorylated at Ser2056 from a patient that experienced progressive disease following combination checkpoint therapy. In contrast, melanoma expressing moderate levels of DNA-PK, but deficient or low levels of phosphorylated DNA-PK demonstrated favorable responses to checkpoint therapy.

***DNA-PKi confers PD-1/CTLA-4 checkpoint blockade efficacy against established B16-F10 melanoma tumors.*** B16-F10 melanoma is an extremely aggressive cell line in part owing to its weak immunogenicity. Combination blockade of CTLA-4 and PD-1 on their own are insufficient for controlling tumor growth (43). As shown in **Figure 1**, a single round of NU-SL40 therapy, in the absence of checkpoint blockade, achieved tumor regression in 100% of mice but this response was transient, and all mice succumbed to the tumor within ~40 days. The standard of care for melanoma patients is combination blockade of CTLA-4 and PD-1 and results in a 5-year overall survival of ~60%. Since the efficacy of checkpoint therapy is linked to the neoantigen load and NU7441 increased neoantigen expression, we investigated the ability for NU-SL40 to enhance the anti-tumor activity of combination treatment with anti-PD-1/-CTLA-4 in

mice bearing an established B16-F10 tumor. Administration of NU-SL40 delayed tumor growth whereas mice treated with checkpoint blockade sustained similar growth kinetics to untreated mice, **Figure 6G**. In sharp contrast, mice treated with NU-SL40 and anti-PD-1/-CTLA-4 exhibited tumor regression in all mice. Despite the association of B16-F10 tumors to promote cachexia in the setting of immunostimulation and robust anti-tumor immune responses, there was no marked variation in mouse weights between treatment groups in our model, **Supplemental Figure S6**.

To determine the role that DNA-PK in cancer cells played in altering their immunogenicity, we knocked-out DNA-PK in B16-F10 melanoma cells (B16-F10$^{\text{DNA-PK KO}}$), **Supplemental Figure S7A and 7B**, and investigated mouse survival and tumor growth in response to checkpoint therapy. In the absence of treatment, DNA-PK deletion had no impact on tumor growth, **Figure 6H, left panel.** However, B16-F10$^{\text{DNA-PK KO}}$ tumors were sensitized to anti-PD-1/CTLA-4 therapy, **Figure 6H, middle panel**. Our data in Figure 1, indicated that including anti-CD40 treatment to activate APCs contributed to generating anti-tumor T cell responses. Thus, we sought to determine whether adding anti-CD40 treatment further improved tumor immunity against B16-F10$^{\text{DNA-PK KO}}$ tumors. As shown in **Figure 6H**, **right panel**, supplementing with anti-CD40 substantially enhanced anti-tumor responses against B16-F10$^{\text{DNA-PK KO}}$ tumors but not control tumors**.** Immunological responses were robust and mice remained tumor-free for 300 days, **Figure 6H** and **6I**. To examine whether this combination treatment induced long-lived T cells capable of controlling a subsequent tumor rechallenge, surviving and a naïve group of mice were injected with B16-F10$^{\text{DNA-PK KO}}$ cells and tumor growth kinetics and survival monitored for 75 days. All surviving mice demonstrated a vigorous anti-tumor response capable of controlling tumor growth, **Figure 6J**. In sharp contrast, all naïve mice succumbed to tumor challenge.

Collectively, these data show that reduced *PRKDC* levels are associated with increased *HLA-A* expression, TIL CD8 expression, and improved response to checkpoint therapy.

Furthermore, inhibiting DNA-PK with a pharmacological inhibitor or knocking it out induces efficacy of checkpoint blockade to a typically immunotherapy-resistant melanoma tumor.

## Discussion

Despite serving as the first line treatment for melanoma, combination therapy with PD-1 and CTLA-4 blockade is ineffective in 40% of treatment-naïve melanoma patients. The lack of durable response or recurrence of tumors demonstrates selective pressures impairing the immune system's recognition and destruction of the tumor leading to the outgrowth of cancer cells with reduced MHC-I expression or limited expression of antigenic epitopes. Collectively, our studies highlight that a) DNA-PKi enhances anti-tumor immune responses by creating a potent inflammatory tumor environment that favors tumor antigen presentation; b) DNA-PKi increases the levels and induces expression of additional neoepitopes which activate a broad panel of neoantigen-reactive T cells with potent tumor-killing activity; c) reduced *PRKDC* (DNA-PK) levels inversely correlates with CD8 tumor infiltration and elevated MHC-I expression, d) mutations in *PRKDC* are associated with higher TMB and neoantigen loads in human melanomas and enhanced responses to checkpoint blockade, and e) knocking out DNA-PK in mouse melanoma tumors conferred sensitivity to checkpoint and sustained tumor regression.

Approaches designed to diversify and increase the neoantigen landscape or to intensify the expression of TAAs are especially relevant to cancers with low TMB including rare melanoma subtypes such as uveal, mucosal, and acral. Neoantigen-reactive T cells play a critical role in destroying tumors in patients receiving checkpoint blockade and ACT (1-3). Studies of lung cancer and melanoma patients undergoing checkpoint blockade therapy highlighted a correlation between response to therapy and the number of tumor somatic mutations (6, 7). These studies also reveal that neoantigen expression is heterogenous; while some neoantigens are clonal and present in most/all cancer cells within the same patient, other neoantigens are sub-clonal and expressed in only a fraction of the cancer cells (8). In our studies, DNA-PKi alone was sufficient to drive the expression of various TAAs and neoantigens. We observed a significant delay in tumor growth in all mice and complete tumor regression in ~37% of mice

515 treated with DNA-PK inhibition plus immune adjuvants, and 100% tumor regression when paired
516 with anti-PD-1/-CTLA-4 blockade. In contrast, none of the mice treated with any other
517 combination of DNA-PKi or checkpoint blockade exhibited tumor regression. These data
518 suggest that diversifying and increasing the expression of neoantigens contributed to the
519 induction of effective T cell mediated tumor immunity. Thus, development of therapies targeting
520 neoantigens can generate tumor-specific immune responses. Moreover, boosting immune
521 responses towards generation of known TAAs is also advantageous as they can be highly
522 expressed across patients. In isolates from TIL, peripheral blood, or lymph nodes (44), the
523 frequency of TAA-specific T cells is higher than that of neoantigen-reactive T cells. Further,
524 whereas neoepitopes and the presence of neoepitope-specific T cells vary amongst patients
525 with a common cancer type, the same TAAs such as MART-1, GP100, TYRP, etc. are routinely
526 expressed in diverse types of cancer (45). Our studies suggest that DNA-PK inhibition is a
527 potential strategy to boost TAA and neoantigen-reactive T cell responses and improve the
528 efficacy of anti-PD-1/-CTLA-4 blockade-based therapies.
529
530 The mechanisms by which DNA-PK inhibition drives the expression of neoantigens and
531 TAAs is not clear. DNA-PK is a serine/threonine protein kinase with a vital role in the DNA
532 damage response and maintenance of genomic stability by mediating ligation of DNA double-
533 strand breaks through nonhomologous end joining (11, 12). However, relevant to our studies,
534 and independent of its role as a DNA repair enzyme, emerging evidence suggests that the
535 DNA-PKcs can play a critical role in transcriptional regulation. For example, Goodwin et al.
536 demonstrated that in prostate cancer, DNA-PK interacted with the androgen receptor (AR) at
537 DNA transcriptional sites where it facilitated AR-dependent transcriptional transactivation (46) of
538 a panel of genes that drive prostate cancer progression. In melanoma, Kotula et al.
539 demonstrated that DNA-PKcs enhanced pro-metastatic activity by promoting the transcription of
540 genes coding for secreted proteins known to modulate tumor migration and invasion (47). Giffin

et al. demonstrated that DNA-PK, via the Ku subunits, binds directly to NRE1 DNA sequence elements within the mouse mammary tumor virus (MMTV) promoter resulting in transcriptional repression (48). DNA-PK has also been demonstrated to bind to the E-box/TATA DNA elements and suppress gene expression (49).

In support of DNA-PK's role as a transcriptional repressor in our model, we find that inhibiting DNA-PK drives neoantigen and TAA expression at the transcriptional level. Further, in patients treated with anti-PD-1/-CTLA-4 blockade therapies, reduced *PRKDC* levels inversely correlates with CD8 TIL and MHC-I expression, and *PRKDC* mutations are associated with higher neoantigen loads and enhanced responses. Based on these reports and in conjunction with our data demonstrating the increased transcription of a variety of genes with neoantigens, our ongoing studies are focused on understanding whether DNA-PK plays a role as a transcriptional repressor and whether blocking this function contributes to the restoration of tumor antigen expression.

The identification of baseline biomarkers to predict clinical outcomes or safety has become a priority for administering cancer immunotherapies. Amongst these biomarkers are CD8 TIL displaying specific inflammatory cytokine profiles. Our data indicates that genes coding for TIL-recruiting-chemokines CXCL9 and CCL5 were amongst the most upregulated genes in NU-SL40-treated mice. Other biomarkers include microsatellite instability status and tumor mutational burden that can serve as a surrogate for the presence of T cell epitopes derived from neoantigens. Our data reveals that in melanoma patients treated with anti-PD-1/-CTLA-4 blockade, *PRKDC* mutations are associated with higher TMB, neoantigen loads, and enhanced responses. Other potential biomarkers associated with the presence of tumor-reactive T cells and response to immunotherapies include proteins that regulate antigen processing and MHC expression (50). Our data indicate that in melanoma patients, reduced *PRKDC* levels correlated

with increased CD8 TIL and MHC-I expression, both of which are strong indicators of response to immunotherapy. Further, H2 family members which participate in antigen processing and presentation by MHC-I and -II were upregulated in response to NU-SL40 treatment. DNA-PKi was previously reported to reduce the expression of PD-L1 and several other immunomodulatory proteins while increasing MHC-I in a heterogeneous panel of melanoma cell lines (9). Finally, the use of IFNγ gene signatures, including the presence of IFNγ in circulation, in the tumor, or relating to the responsiveness of tumors to IFNγ have also been suggested to be relevant biomarkers. Our studies demonstrate that administration of a DNA-PKi in conjunction with immune adjuvants strongly induces a clinically relevant IFNγ and inflammatory gene signature favoring tumor antigen processing and presentation, and T cell recruitment. We propose that the DNA-PK transcript or protein levels, or the presence of mutations in *PRKDC* alone or in combination with existing biomarkers could improve the use of predictive indicators of response to T cell-based cancer immunotherapies.

Through these studies, we propose that DNA-PK inhibition plays an alternate role as an immune-modifying agent through its ability to promote an inflammatory tumor environment and positively impact neoantigen load and TAA expression. In concert with its ability to promote antigen processing, DNA-PK inhibition can broaden the repertoire of neoantigen-reactive T cells with heightened anti-tumor activity. Numerous compounds are in clinical testing to evaluate the efficacy of targeting DNA-PK [NCT02516813, NCT02316197, NCT01353625, and NCT02833883] and could offer the opportunity to design clinical trials around the concept of inhibiting DNA-PK activity to promote tumor immunogenicity in the setting of therapy resistant tumors.

## Methods

*Sex as a biological variable.* Our study analyzed data from male and female patients and used male and female mice.

*Cell Culture.* B16-F10 cells (CRL-6475, ATCC) were cultured as recommended by ATCC. For in vitro experiments, B16-F10 cells with 70% confluency were stimulated with 100U/mL recombinant mouse IFNγ (575304, Biolegend) 16-20 hours before collection. DC2.4 murine dendritic cells (32011203, Sigma) were cultured in RPMI 1640 supplemented with 1X L-glutamine (TMS-002-C, Sigma), 1X NEAA (TMS-001-C, Sigma), 1X HEPES (15630080, Gibco), 0.0054x β-mercaptoethanol (ES-007-E, Sigma). Isolated TIL and PBMC were cultured in TIL media (RPMI 1640 supplemented with 10% Fetal Bovine Serum, 1% Penicillin-Streptomycin (15070063, ThermoFisher), 50U/mL IL-2 (NDC 65483-116-07, Proleukin (aldesleukin)), 50mM β-mercaptoethanol). Cell lines were evaluated for mycoplasma weekly. Adherent cell lines were harvested with 0.25% Trypsin/EDTA (25200056, ThermoFisher). All cells were cultured at 37°C, 7% $CO_2$.

*Animal Model*. C57BL/6J mice (The Jackson Laboratory–JAX, #000664) between 8-10 weeks were used for all experiments involving B16-F10 melanoma cell injections. Mice were humanely euthanized using compressed $CO_2$ air for primary euthanasia and cardiac perfusion or cervical dislocation for secondary methods.

*Therapeutics.* NU7441 (S2638-05, SelleckChem; HY-11006 5mg, MedChemExpress) was reconstituted in warm DMSO at 12.5mg/mL creating 10X aliquots then diluted to 1X at 1.25mg/mL with 5% Kolliphor (C5135-500G, Sigma) in saline. STING ligand (DMXAA - tlrl-dmx, Invivogen) was reconstituted in DMSO at 10mg/mL creating 2X STGL aliquots then diluted to 1X in molecular-grade $H_2O$ to 5mg/mL. Anti-CD40 antibody (BE0016-2, BioXCel) was

suspended at 1mg/mL in sterile saline. Anti-CD8 depletion antibody (clone 53-6.7; BioXcell) was suspended at 1mg/mL in PBS.

*In Vivo Tumor Model and Drug Treatment.* 8–10-week-old mice were injected subcutaneously at the flank, lateral to midline with $2x10^5$/100µL of B16-F10 melanoma cells in 0.1% FBS in PBS. For DNA-PKi alone and NU-SL40 combination, NU7441 was given 2x/day (9 hours between treatments) for five days intraperitoneally (i.p.) in 100µL (0.125mg/mouse/injection) when tumors were ~25$mm^2$. When tumors reached ~40$mm^2$, STING ligand was administered one time intratumorally (i.t.) in 10µL (50µg/mouse). In vivo mouse anti-CD40 antibody was administered in conjunction with STING ligand injections one-time (i.p.) in 100µL (100µg/mouse). For SL40-NU, SL40 was administered when tumors reached ~40$mm^2$ , followed by five days of NU7441. For CD8 depletion, mice were injected (i.p) with 100µL (100µg/mouse) of anti-CD8 antibody at four and two days prior to SL40 injections. Mice were euthanized and tumors were harvested 7-9 days from the initiation of NU7441 treatment.

*Tumor and Lymph Nodes.* B16-F10 tumors and draining inguinal lymph nodes were extracted and mechanically digested through a 70µM strainer into Wash Buffer (HBSS, 5mM EDTA, 2% FBS). The tumor single-cell suspension was then resuspended at 10mL/gram of tissue in Digestion Buffer (RPMI 1640, 2U TURBO™ DNase (AM2238, Invitrogen),100µL Liberase DH (5401054001, Sigma)). The tumor suspension was incubated and rocked at 37°C for 30 minutes then poured through a 40µM strainer.

*Blood and Spleen.* Blood was collected via cardiac perfusion secondary euthanasia method and spleens were extracted. Blood was collected in LH Lithium Heparin tubes (450477, Greiner Bio-One) and held on ice. Spleen was mechanically processed through a 70µM strainer into Wash Buffer. Blood and spleen pellets were resuspended in 1X RBC Lysis Buffer (420301, Biolegend)

for 2 minutes and quenched with PBS then prepared for antibody staining or resuspended in 1ml of TIL media and plated in a 48-well plate for incubation overnight.

*Serum.* Blood was collected into microcentrifuge tubes, held on ice while coagulating for 75 minutes followed by centrifugation at 2000rpm for 10 minutes to isolate serum. Serum was stored at -80°C.

*RNA Extraction from Tumor Tissue.* Tumor tissue (<1 gram) was placed into RNase free microcentrifuge tubes without buffer, on ice. Tumor cells were lysed, and RNA/DNA were extracted from tissue using Qiagen RNeasy Mini Kit (74104). Sample concentration and purity were determined using NanoDrop One/OneC and RNA integrity was further validated using RNA ScreenTape for the Agilent 2200 TapeStation (5067-5576, Agilent Technologies).

*Ex Vivo Isolated TIL B16-F10 Rechallenge.* TIL from digested single-cell tumor suspension were isolated using mouse CD4, CD8 (TIL) MicroBeads (130-116-480, Miltenyi) and LS columns (130-042-401, Miltenyi) per the manufacturers protocol. TIL were suspended in TIL media and cultured in a 96-well plate alone or with stimulated B16-F10 cells (1:1 ratio, 200K total/200µL per well) for 20 hours for surface/intracellular staining. Supernatant was collected at 14 hours followed by Golgi Stop (BD) incubation for 6 hours. Detailed procedure at protocol.io.

*Nanostring Gene Expression.* Samples were prepared for RNA hybridization by diluting RNA to 15ng/µL in RNase-free water. Nanostring Gene Expression CodeSet RNA Hybridization protocol was followed to hybridize RNA to the nCounter Mouse PanCancer IO 360 Panel Codeset (XT-CS0-MIO360-12, NanoString) and run on nCounter Sprint. Samples were analyzed using nSolver and ROSALIND® (https://rosalind.bio/) analysis platforms with

normalized fold changes and p-values as described in the nCounter® Advanced Analysis 2.0 User Manual.

*Melanoma Tumor Antigen Expression.* RNA transcript and protein expression of selected tumor associated antigens was determined in mouse and human melanoma cells by RT-PCR or western blot. $5x10^5$ cells were treated with 4μM NU7441 in 6-well plates and harvested 48-72 hours later.

*Immunohistochemistry.* Tissues stained with establish protocols at University of Colorado Histology Core using DNA-PK (Cell Signaling #12311) Rabbit mAb 1:100, p-DNA-PK (Abcam #ab18192) Rabbit polyclonal 1:200.

*Neoantigen Identification and Tandem Mini Gene Neoantigen Plasmid Generation.* Neoantigens were determined as previously described (37). B16-F10 cells were treated in tissue culture with 2.5μM NU7441 for 48 hours at which time RNA and genomic DNA were extracted. As controls, RNA and genomic DNA were extracted from the spleens of C57BL/6 mice. WES data were analyzed by the standard Exome Variant Detection pipeline on Partek Flow platform (v9.0.20.0819) and aligned with mouse genome database (mm10) by BWA (v0.7.12). We used three variant callers (FreeBayes (v1.0.1), Strelka (v1.0.15), and GATK Mutect2 (v4.0)). Spleen DNA sample served as the normal control. Variants shared with spleen were considered as SNP and removed. RNA FKPM levels of tumor associated antigens and neoantigens show the extent of upregulation.

*DC2.4 Tandem Mini Gene Neoantigen Plasmid Nucleofection and ex vivo TIL Stimulation.* DC2.4 cells were cultured for 48 hours in DC2.4 media to reach 80-90% confluency and collected for nucleofection with one of 10 tandem-mini genes (TMG) or a control GFP plasmid

using Cell Line Nucleofector Kit L (VCA-1005, Lonza). 2µg of TMG or GFP plasmid DNA was nucleofected using program Y-001, following the protocol for Immature and Mature Mouse Dendritic Cells. Transfection efficiency ranged between 65-80%. Each TMG-DC2.4 sample was resuspended in TIL media with 50U/mL IL-2 and plated in a 96-well plate at a 10:1 ratio of TIL to DC and cultured overnight at 37°C. The production of IFNγ and granzyme B was determined by flow cytometry or ELISA.

*ELISA.* Supernatant samples stored at -20°C and thawed on ice then diluted 1:5 for mouse IFNγ ELISA (430804, Biolegend) and plated in triplicate. $OD_{450}$ and $OD_{570}$ readings were obtained; $OD_{570}$ values were subtracted from $OD_{450}$, triplicate samples were averaged, and standard curve used to determine pg/mL concentrations. Final IFNγ concentration was determined by multiplying pg/mL concentration by dilution factor.

*Antibody Staining and Flow Cytometry.* The following surface and intracellular staining panels were used to assess surface TCR expression, functional capacity of TIL, lymphoid/myeloid tumor distribution and functional response to TMG-DCs. BD Cytofix/Cytoperm Kit with GolgiStop (554715) was used for intracellular staining. Samples were acquired with Cytek Aurora 3L Plate Loader and analyzed in FlowJo. For cell surface staining and functional assays: Biolegend – Zombie Aqua (#423102), BV650 CD3 (17A2, #100229), Alexa Fluor 700 CD4 (RM4-4, #116022), APC-Cy7 CD8 (53-6.7, #100714), PE 4-1BB (17B5, #106105), APC 4-1BB (17B5, #106110), PE-Cy7 PD-1 (29F.1A12, #135216), APC CD206 (C068C2, #141707), PE-Cy7 F4/80 (BM8, #123113), PerCp-Cy5.5 CD38 (90, #102722), BV421 Granzyme B (QA18A28, #396414), BV711 CD107a (1D4B, #121614), . For TIL plus DC studies. PerCP CD8a (53-6.7, #100732), PE TCRvβ6 (RR4-7, #140004), PE TCRvβ8.3 (1B3.3, #156304), PE-Cy7 IFNγ (XMG1.2, #505826), BV421 Granzyme B (QA18A28, #396414), BV785 CD3 (17A2, #100231), APC Perforin (S16009A, #154304), PerCp-Cy5.5 TNFα (MP6-XT22, #506322). For

Lymphoid/Myeloid Panels: Zombie Aqua (#423102), APC/Fire-750 CD45 (30-F11, #103153), BV785 CD3 BV785 CD3 (17A2, #100231), Alexa Fluor 700 CD4 (RM4-4, #116022), FITC CD8α (5H10-1, #100803), BV605 TCR γ/δ (GL3, #118129), PE CD20 (SA271G2, #152105), APC NK1.1 (S17016D, #156505), APC/Fire-810 F4/80 (BM8, #123165), BV650 GR-1 (RB6-8C5, #108441), BV711 CD206 (C068C2, #141727), PE-Cy7 CD11b (M1/70, 101215), PE/Dazzle-594 CD11c (N418, #117347), PerCP I-A/I-E (M5/114.15.2, #107623). BD Biosciences – BV480 TCRvβ9 (MR10-2, #746449), BV480 TCRvβ10[b] (B21.5, #746729), BV650 TCRvβ11 (RR3-15, #743679), BV650 TCRvβ13 (MR12-3, #743993), BV711 TCRvβ2 (B20.6, #745428), BV711 TCRvβ3 (KJ25, #743416), BV785 TCRvβ5.1,5.2 (MR9-4, #743003), BV785 TCRvβ 8.1,8.2 (MR5-2, #744334), FITC TCRvβ7 (TR310, #553215), FITC TCRvβ14 (14-2, #553258), BV480 CD45.1 (A20, #746666), anti-Vβ FITC TCR kit (557004). Detailed reagents, panels, procedure, and FlowJo analysis strategy at protocol.io.

*TCGA Data Collection and Analysis.* The publicly available TCGA datasets from melanoma patients were directly downloaded from the TCGA Data Portal at https://tcga-data.nci.nih.gov/tcga/.

*Study Approval*. All mice were housed at, and all animal procedures were approved by University of Colorado Anschutz Medical Campus's Institutional Animal Care and Use Committee (IACUC).

*Statistics.* Nanostring data was analyzed with nSolver, and Rosalind software and statistically significant changes identified as p-values less than 0.05 and fold changes greater than ± 1.5. Remaining analysis completed with GraphPad Prism software. Differences between treatment groups are determined by two-way ANOVA. Differences between TCRvβ groups determined by

multiple unpaired two-tailed t-tests relative to untreated control. Differences between patient groups from TCGA data determined by unpaired Mann-Whitney test.

*Data Availability Statement*

The data generated in this study are available upon request from the corresponding author.

**Author contributions.** E.D., A.J.N., G.K.A., designed the research studies. A.J.N., G.K.A., A.S., J.C., J.L, A.S.D., D.G., and X.B. conducted experiments, acquired, and analyzed data. E.D., A.J.N., G.K.A, A.B.W., wrote and/or edited the manuscript. W.R., M.M., R.T., A.M., K.C., provided reagents and patient samples. E.D., G.K.A., J.D.H., A.M., K.C., acquired and analyzed genetic data.

**Acknowledgments**

Studies were supported by grants from the National Cancer Institute R01CA271537, R01CA207913, and P30CA046934, the Department of Veteran Affairs, BX004935-01, and the University of Colorado Comprehensive Cancer Center.

## References


1. Rizvi NA, Hellmann MD, Snyder A, Kvistborg P, Makarov V, Havel JJ, et al. Cancer immunology. Mutational landscape determines sensitivity to PD-1 blockade in non-small cell lung cancer. *Science.* 2015;348(6230):124-8.
2. Snyder A, Makarov V, Merghoub T, Yuan J, Zaretsky JM, Desrichard A, et al. Genetic basis for clinical response to CTLA-4 blockade in melanoma. *N Engl J Med.* 2014;371(23):2189-99.
3. Lauss M, Donia M, Harbst K, Andersen R, Mitra S, Rosengren F, et al. Mutational and putative neoantigen load predict clinical benefit of adoptive T cell therapy in melanoma. *Nat Commun.* 2017;8(1):1738.
4. Huang J, El-Gamil M, Dudley ME, Li YF, Rosenberg SA, and Robbins PF. T cells associated with tumor regression recognize frameshifted products of the CDKN2A tumor suppressor gene locus and a mutated HLA class I gene product. *J Immunol.* 2004;172(10):6057-64.
5. Linnemann C, van Buuren MM, Bies L, Verdegaal EM, Schotte R, Calis JJ, et al. High-throughput epitope discovery reveals frequent recognition of neo-antigens by CD4+ T cells in human melanoma. *Nat Med.* 2015;21(1):81-5.
6. Lee W, Jiang Z, Liu J, Haverty PM, Guan Y, Stinson J, et al. The mutation spectrum revealed by paired genome sequences from a lung cancer patient. *Nature.* 2010;465(7297):473-7.
7. Berger MF, Hodis E, Heffernan TP, Deribe YL, Lawrence MS, Protopopov A, et al. Melanoma genome sequencing reveals frequent PREX2 mutations. *Nature.* 2012;485(7399):502-6.
8. McGranahan N, Furness AJ, Rosenthal R, Ramskov S, Lyngaa R, Saini SK, et al. Clonal neoantigens elicit T cell immunoreactivity and sensitivity to immune checkpoint blockade. *Science.* 2016;351(6280):1463-9.

9. Tsai AK, Khan AY, Worgo CE, Wang LL, Liang Y, and Davila E. A Multikinase and DNA-PK Inhibitor Combination Immunomodulates Melanomas, Suppresses Tumor Progression, and Enhances Immunotherapies. *Cancer Immunol Res.* 2017;5(9):790-803.
10. Guo J, Muse E, Christians AJ, Swanson SJ, and Davila E. An Anticancer Drug Cocktail of Three Kinase Inhibitors Improved Response to a Dendritic Cell-Based Cancer Vaccine. *Cancer Immunol Res.* 2019;7(9):1523-1534.
11. Blackford AN, and Jackson SP. ATM, ATR, and DNA-PK: The Trinity at the Heart of the DNA Damage Response. *Mol Cell.* 2017;66(6):801-17.
12. Yoo S, and Dynan WS. Geometry of a complex formed by double strand break repair proteins at a single DNA end: recruitment of DNA-PKcs induces inward translocation of Ku protein. *Nucleic Acids Res.* 1999;27(24):4679-86.
13. Kono M, Dunn IS, Durda PJ, Butera D, Rose LB, Haggerty TJ, et al. Role of the mitogen-activated protein kinase signaling pathway in the regulation of human melanocytic antigen expression. *Mol cancer res.* 2006;4(10):779-92.
14. Boni A, Cogdill AP, Dang P, Udayakumar D, Njauw CN, Sloss CM, et al. Selective BRAFV600E inhibition enhances T-cell recognition of melanoma without affecting lymphocyte function. *Cancer res.* 2010;70(13):5213-9.
15. Frederick DT, Piris A, Cogdill AP, Cooper ZA, Lezcano C, Ferrone CR, et al. BRAF inhibition is associated with enhanced melanoma antigen expression and a more favorable tumor microenvironment in patients with metastatic melanoma. *Clincancer res.* 2013;19(5):1225-31.
16. Voltarelli FA, Frajacomo FT, Padilha CDS, Testa MTJ, Cella PS, Ribeiro DF, et al. Syngeneic B16F10 Melanoma Causes Cachexia and Impaired Skeletal Muscle Strength and Locomotor Activity in Mice. *Front Physiol.* 2017;8715.

17. Hwang S, Kwon AY, Jeong JY, Kim S, Kang H, Park J, et al. Immune gene signatures for predicting durable clinical benefit of anti-PD-1 immunotherapy in patients with non-small cell lung cancer. *Sci Rep-Uk.* 2020;10(1):643.
18. Chen HQ, Lin RX, Lin WB, Chen Q, Ye DJ, Li J, et al. An immune gene signature to predict prognosis and immunotherapeutic response in lung adenocarcinoma. *Sci Rep-Uk.* 2022;12(1):8230.
19. Auslander N, Zhang G, Lee JS, Frederick DT, Miao B, Moll T, et al. Robust prediction of response to immune checkpoint blockade therapy in metastatic melanoma (vol 24, pg 1545, 2018). *Nat Med.* 2018;24(12):1942.
20. Wang QQ, Wang XK, Liang Q, Wang SJ, Liao XW, Pan FQ, et al. Distinct prognostic value of mRNA expression of guanylate-binding protein genes in skin cutaneous melanoma. *Oncol Lett.* 2018;15(5):7914-22.
21. Zainulabadeen A, Yao P, and Zare H. Underexpression of Specific Interferon Genes Is Associated with Poor Prognosis of Melanoma. *PLoS One.* 2017;12(1):e0170025.
22. Karin N. CXCR3 Ligands in Cancer and Autoimmunity, Chemoattraction of Effector T Cells, and Beyond. *Front Immunol.* 2020;11:976.
23. Yarlagadda K, Hassani J, Foote IP, and Markowitz J. The role of nitric oxide in melanoma. *Biochim Biophys Acta Rev Cancer.* 2017;1868(2):500-9.
24. Lin X, Sun R, Zhao X, Zhu D, Zhao X, Gu Q, et al. C-myc overexpression drives melanoma metastasis by promoting vasculogenic mimicry via c-myc/snail/Bax signaling. *J Mol Med (Berl).* 2017;95(1):53-67.
25. Beleaua MA, Jung I, Braicu C, Milutin D, and Gurzu S. SOX11, SOX10 and MITF Gene Interaction: A Possible Diagnostic Tool in Malignant Melanoma. *Life.* 2021;11(4):281.
26. Fu XQ, Liu B, Wang YP, Li JK, Zhu PL, Li T, et al. Activation of STAT3 is a key event in TLR4 signaling-mediated melanoma progression. *Cell Death Dis.* 2020;11(4):246.

27. Riker AI, Enkemann SA, Fodstad O, Liu S, Ren S, Morris C, et al. The gene expression profiles of primary and metastatic melanoma yields a transition point of tumor progression and metastasis. *BMC Med Genomics.* 2008;1:13.
28. Wu X, Wang X, Zhao Y, Li K, Yu B, and Zhang J. Granzyme family acts as a predict biomarker in cutaneous melanoma and indicates more benefit from anti-PD-1 immunotherapy. *Int J Med Sci.* 2021;18(7):1657-69.
29. Li XY, Corvino D, Nowlan B, Aguilera AR, Ng SS, Braun M, et al. NKG7 Is Required for Optimal Antitumor T-cell Immunity. *Cancer Immunol Res.* 2022;10(2):154-61.
30. Inozume T, Hanada K, Wang QJ, Ahmadzadeh M, Wunderlich JR, Rosenberg SA, et al. Selection of CD8+PD-1+ lymphocytes in fresh human melanomas enriches for tumor-reactive T cells. *J Immunother.* 2010;33(9):956-64.
31. Ye Q, Song DG, Poussin M, Yamamoto T, Best A, Li C, et al. CD137 accurately identifies and enriches for naturally occurring tumor-reactive T cells in tumor. *Clin Cancer Res.* 2014;20(1):44-55.
32. Valpione S, Mundra PA, Galvani E, Campana LG, Lorigan P, De Rosa F, et al. The T cell receptor repertoire of tumor infiltrating T cells is predictive and prognostic for cancer survival (vol 12, 4098, 2021). *Nat Commun.* 2021;12(1):4098.
33. Van Allen EM, Miao D, Schilling B, Shukla SA, Blank C, Zimmer L, et al. Genomic correlates of response to CTLA-4 blockade in metastatic melanoma. *Science.* 2015;350(6257):207-11.
34. Riaz N, Havel JJ, Makarov V, Desrichard A, Urba WJ, Sims JS, et al. Tumor and Microenvironment Evolution during Immunotherapy with Nivolumab. *Cell.* 2017;171(4):934-49 e16.
35. Lucca LE, Axisa PP, Lu B, Harnett B, Jessel S, Zhang L, et al. Circulating clonally expanded T cells reflect functions of tumor-infiltrating T cells. *J ExpMed.* 2021;218(4)e20200921.

36. Postow MA, Manuel M, Wong P, Yuan J, Dong Z, Liu C, et al. Peripheral T cell receptor diversity is associated with clinical outcomes following ipilimumab treatment in metastatic melanoma. *J Immunother Cancer.* 2015;3:23.
37. Slominski RM, Sarna T, Plonka PM, Raman C, Brozyna AA, and Slominski AT. Melanoma, Melanin, and Melanogenesis: The Yin and Yang Relationship. *FrontOnc.* 2022;12:842496.
38. Castle JC, Kreiter S, Diekmann J, Lower M, van de Roemer N, de GJ, et al. Exploiting the mutanome for tumor vaccination. *Cancer Res.* 2012;72(5):1081-91.
39. Lu YC, Yao X, Crystal JS, Li YF, El-Gamil M, Gross C, et al. Efficient identification of mutated cancer antigens recognized by T cells associated with durable tumor regressions. *Clin Cancer Res.* 2014;20(13):3401-10.
40. Lu YC, Zheng Z, Robbins PF, Tran E, Prickett TD, Gartner JJ, et al. An Efficient Single-Cell RNA-Seq Approach to Identify Neoantigen-Specific T Cell Receptors. *Mol Ther.* 2018;26(2):379-89.
41. McGrail DJ, Pilie PG, Rashid NU, Voorwerk L, Slagter M, Kok M, et al. High tumor mutation burden fails to predict immune checkpoint blockade response across all cancer types. *Annals of Oncology.* 2021;32(5):661-72.
42. Tan KT, Yeh CN, Chang YC, Cheng JH, Fang WL, Yeh YC, et al. PRKDC: new biomarker and drug target for checkpoint blockade immunotherapy. *J Immunother Cancer.* 2020;8(1):e000485.
43. Curran MA, Montalvo W, Yagita H, and Allison JP. PD-1 and CTLA-4 combination blockade expands infiltrating T cells and reduces regulatory T and myeloid cells within B16 melanoma tumors. *Proc Natl Acad Sci USA.* 2010;107(9):4275-80.
44. Cheever MA, Allison JP, Ferris AS, Finn OJ, Hastings BM, Hecht TT, et al. The prioritization of cancer antigens: a national cancer institute pilot project for the acceleration of translational research. *Clin Cancer Res.* 2009;15(17):5323-37.

45. Schumacher TN, and Schreiber RD. Neoantigens in cancer immunotherapy. *Science.* 2015;348(6230):69-74.
46. Goodwin JF, Kothari V, Drake JM, Zhao S, Dylgjeri E, Dean JL, et al. DNA-PKcs-Mediated Transcriptional Regulation Drives Prostate Cancer Progression and Metastasis. *Cancer Cell.* 2015;28(1):97-113.
47. Kotula E, Berthault N, Agrario C, Lienafa MC, Simon A, Dingli F, et al. DNA-PKcs plays role in cancer metastasis through regulation of secreted proteins involved in migration and invasion. *Cell Cycle.* 2015;14(12):1961-72.
48. Giffin W, Kwast-Welfeld J, Rodda DJ, Prefontaine GG, Traykova-Andonova M, Zhang Y, et al. Sequence-specific DNA binding and transcription factor phosphorylation by Ku Autoantigen/DNA-dependent protein kinase. Phosphorylation of Ser-527 of the rat glucocorticoid receptor. *J Biol Chem.* 1997;272(9):5647-58.
49. Xu P, LaVallee PA, Lin JJ, and Hoidal JR. Characterization of proteins binding to E-box/Ku86 sites and function of Ku86 in transcriptional regulation of the human xanthine oxidoreductase gene. *J Biol Chem.* 2004;279(16):16057-63.
50. Kalaora S, Lee JS, Barnea E, Levy R, Greenberg P, Alon M, et al. Immunoproteasome expression is associated with better prognosis and response to checkpoint therapies in melanoma. *Nat Commun.* 2020;11(1):896.

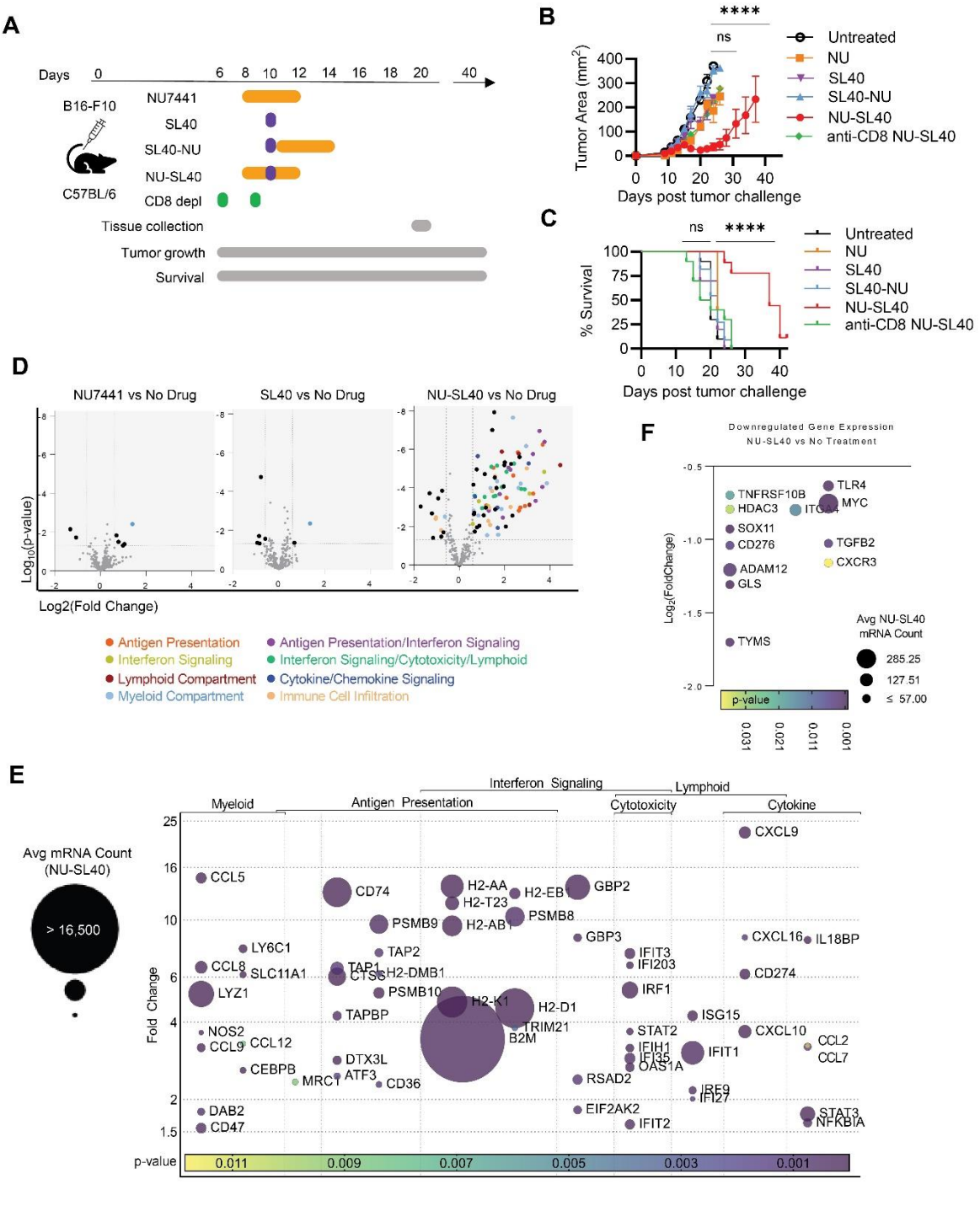


**Figure 1 – Combination immunotherapy with DNA-PK inhibition demonstrates potent anti-tumor CD8 T cell response and is associated with a favorable antigen processing and inflammatory gene expression profile.**

**Figure 1 – Combination immunotherapy with DNA-PK inhibition demonstrates potent anti-tumor CD8 T cell response and is associated with a favorable antigen processing and inflammatory gene expression profile.** A) Model depicting treatment schema. C57BL/6 mice with established ($25mm^2$) B16-F10 tumors underwent the treatment plans shown in A with B) tumor growth and C) survival monitored for 40 days. D-E) Mice with established tumors were treated as described in A and tumors were collected between 7-9 days post initiating treatment. Volcano plots displaying Log2(fold-change) in B16-F10 total tumor mRNA transcript expression comparing treatment relative to no treatment and the associated Log10(p-values) generated by Nanostring gene expression analysis from 3 tumors NU, SL40, and no drug and and 4 tumors from NU-SL40. Genes are colored by pathway association shown in panel D. D and E) Bubble plots depict fold-change in gene expression from NU-SL40-treated tumors from pathways highlighted in volcano plots to be upregulated or downregulated compared to the untreated group. Bubble size represents average mRNA transcript counts in NU-SL40 replicates. The p-value (as compared to untreated) is depicted by color scale.

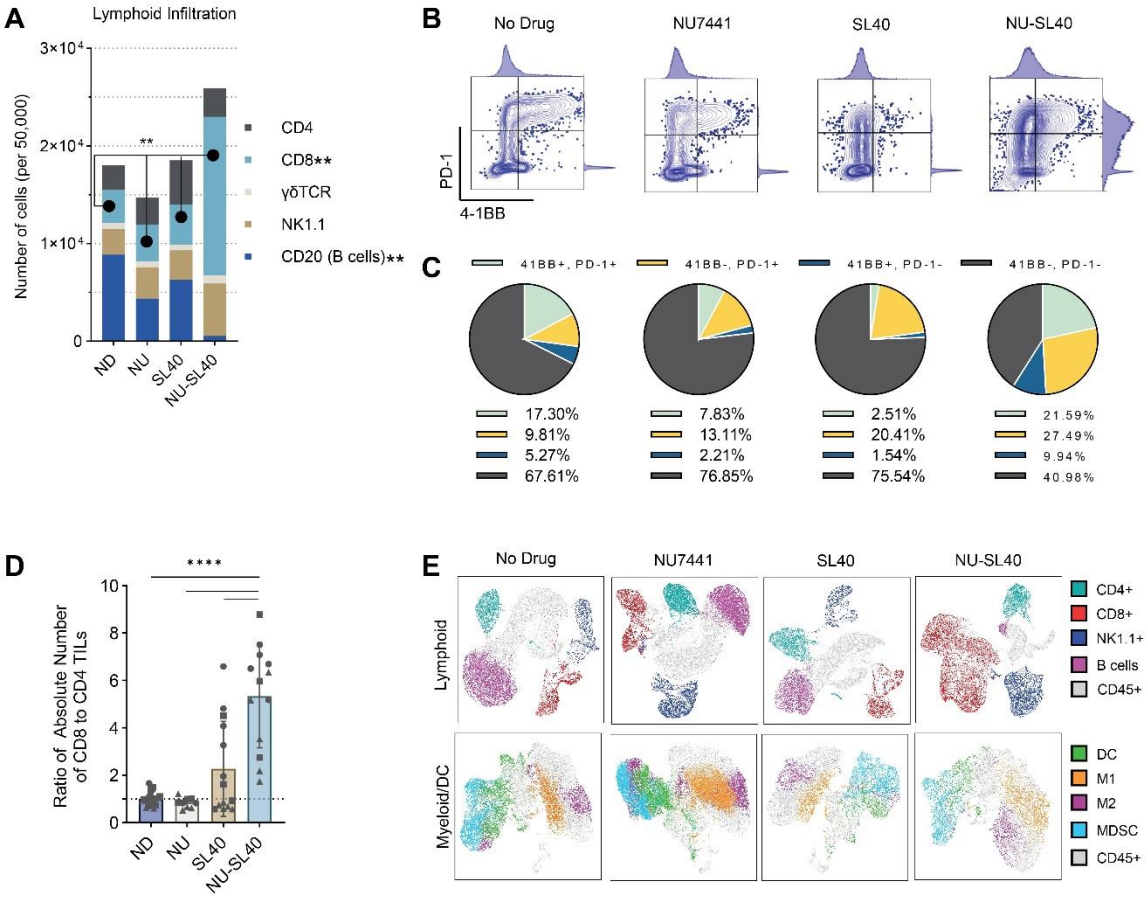


**Figure 2 – NU-SL40 treatment promotes infiltration of activated CD8 TIL and alters the tumor myeloid cell compartment.**

960

961

**Figure 2 – NU-SL40 treatment promotes infiltration of activated CD8 TIL and alters the tumor myeloid cell compartment.** A) Mice with established tumors were treated as described in Figure 1A. The indicated tumor lymphoid cell populations of single-cell, viable, CD3+ or CD3- CD45+ cells normalized to 50,000 CD45+ cells were determined by flow cytometry. Significance determined by two-way ANOVA. (No Drug: n=6, SL40: n=5, NU: n=4, NU-SL40: n=5). B) Representative flow plots with adjunct MFI histograms and C) pie charts representing percent of CD8+ TIL expressing PD-1 and/or 4-1BB across treatment groups (No Drug: n=5, SL40: n=5, NU: n=4, NU-SL40: n=4). D) The ratio of CD8+ to CD4+ TIL. Significance determined by two-way ANOVA. (No Drug: n=20, SL40: n=14, NU: n=9, NU-SL40: n=13). E) UMAP analysis of pooled single-cell, viable, CD45+ TIL populations (top panel) described in A-C (CD4, CD8, NK1.1, B cells) and (bottom panel) M1- or M2-like macrophages identified as $CD45^+F4/80^+CD11c^+CD206^-$ or $CD45^+F4/80^+CD11c^-CD206^-$; $F4/80^+CD45^+CD11c^-CD206^+$; MDSC, $CD11b^+Gr1^+$; DC, $CD45^+CD11c^+MHCII^+$ (No Drug: n=6, SL40: n=5, NU: n=4, NU-SL40: n=5). * $p<0.05$, ** $p<0.01$, *** $p<0.001$, **** $p<0.0001$.

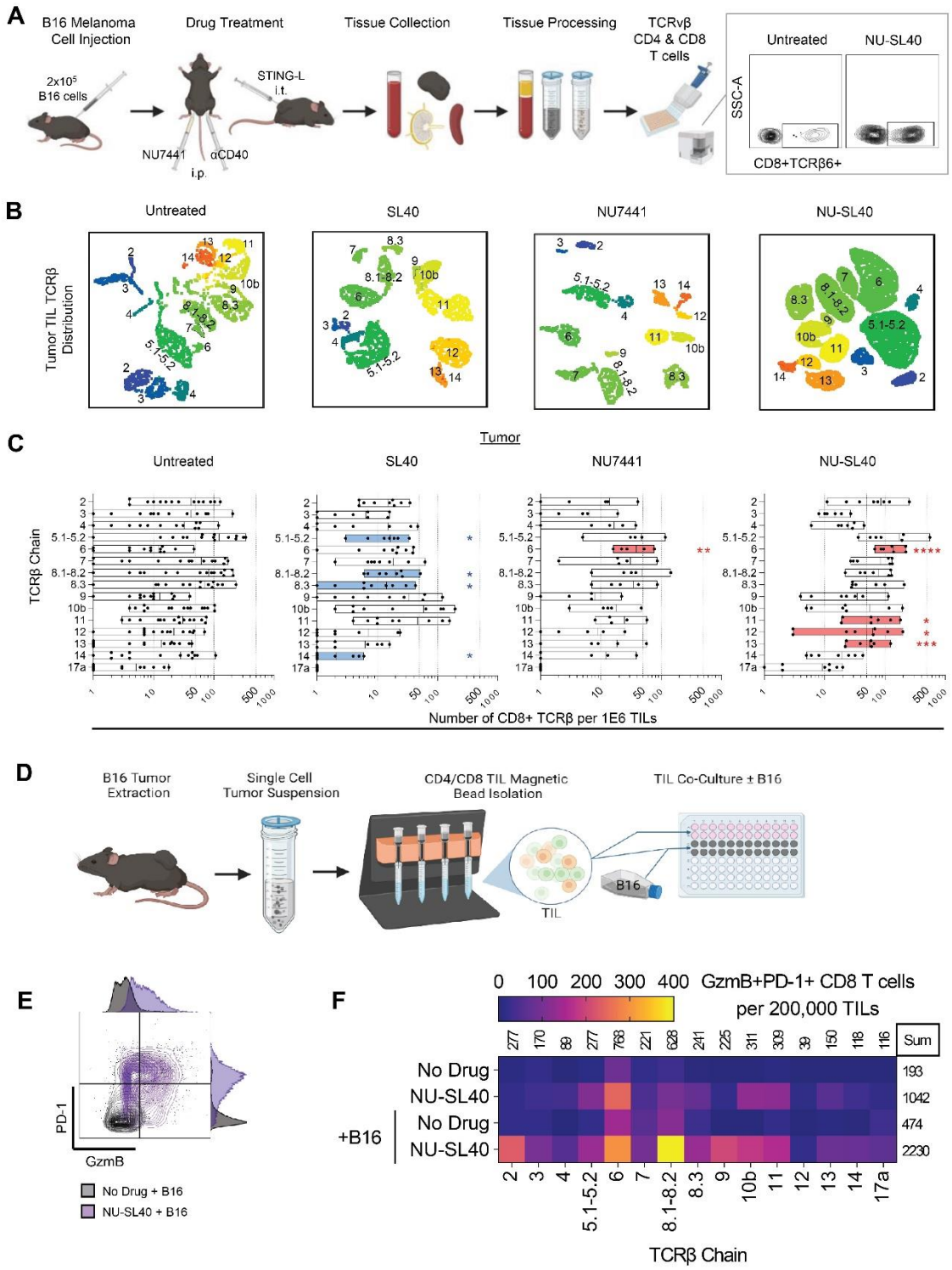


**Figure 3 – DNA-PK inhibition drives TCRvβ diversity of highly functional tumor-reactive CD8 T cells.**

**Figure 3 – DNA-PK inhibition drives TCRvβ diversity of highly functional tumor-reactive CD8 T cells.** A) Schematic of drug treatment and tissue processing with representative flow cytometry analysis of TCRvβ on CD8 TILs. B) UMAP distribution of the absolute number of CD8 TIL clustered by TCRvβ chain (number label, color scale for differentiation) (Untreated: n=15, SL40: n=9, NU: n=5, NU-SL40: n=8). C) Number of CD8+ TIL by TCRvβ chain per 1 million single cell events. Rout outlier test was performed. Blue and red bars represent significant decreases or increases in TCRvβ counts in treatment conditions compared to no treatment. Each dot represents one mouse (Untreated: n=15, SL40: n=9, NU: n=5, NU-SL40: n=8). D) Schematic of C57BL/6 B16-F10 tumor model and tumor collection for TIL isolation via magnetic bead positive selection followed by ex vivo culture with or without IFNγ pre-treated (100U/mL for 24 hours) B16-F10 melanoma cells. E) Representative flow plot with adjunct MFI histograms representing the number of isolated CD8+ TIL expressing GzmB and PD-1 from control and NU-SL40-treated mice (16-hour co-culture). F) Heatmap of TCRvβ distribution of CD8+ TILs that express PD-1 and produce GzmB. TIL were pooled from tumors (Untreated: n=4, NU-SL40: n=5) and counts were normalized to $2x10^5$ CD3+ cells. Sum of TCRvβ chain in each condition is represented above columns, sum of total TCRvβ in each condition indicated to the right of each row. Statistical significance was determined by multiple unpaired t-tests. * $p<0.05$, ** $p<0.01$, *** $p<0.001$, **** $p<0.0001$.

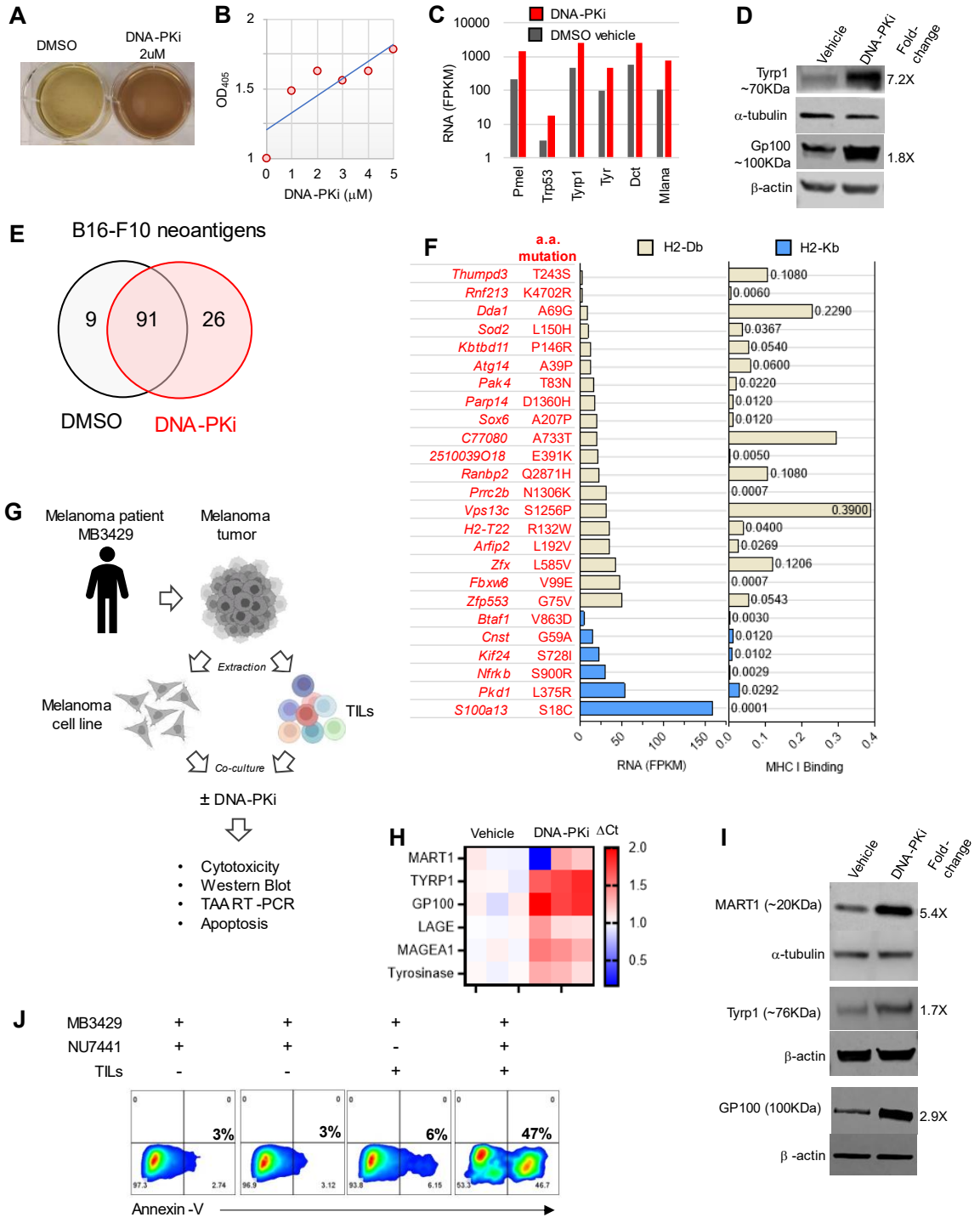


**Figure 4 – DNA-PK inhibition increases tumor associated antigen expression levels, induces a unique neoantigen expression profile in melanoma, and represents better targets for human TILs.**

**Figure 4 – DNA-PK inhibition increases tumor associated antigen expression levels, induces a unique neoantigen expression profile in melanoma, and represents better targets for human TIL.** A-B) B16-F10 melanoma cells were treated with 2μM NU7441 (right) or DMSO control (left) for 72 hours at which point gradual darkening was observed and $OD_{405}$ recorded. C) Bar graph comparing levels of RNA per FPKM of known melanogenesis associated antigens at 48 hours post treatment with 2μM NU7441 or DMSO control. Fold change between DMSO and NU7441 noted above bars. D) B16-F10 melanoma cells were treated with 2μM NU7441 (right) or DMSO control (left) for 48 hours and the levels of the indicated proteins were determined by western blot. Fold-change between groups is shown below each band. E-F) B16-F10 melanoma cells were treated as described in panel A and the neoantigens and FPKM determined as described in the materials and methods section. E) Venn-diagram representing the number of uniquely expressed or shared B16-F10 neoantigens present in control-treated melanoma and those induced by NU7441. F) The gene name and amino acid mutation expressed following DNA-PKi treatment are shown to the left. The matched bar graph shows the levels of RNA per FPKM of neoantigen producing genes exposed by NU7441 treatment as well the binding affinity of these epitopes to H2-Db and H2-Kb determined using IEDB's MHC binding prediction algorithms (iedb.org). G) Schematic showing the generation of melanoma cell lines and TIL from a patient melanoma tumors and experiments performed in panels H-J. H) MB3429 melanoma cell line was treated with 2μM NU7441 or DMSO control for 48 hours and the levels of the indicated transcripts were determined by RT-PCR and shown as Delta Ct. I) MB3429 melanoma cells were treated with 2μM NU7441 or DMSO controls for 48 hours and the levels of the indicated proteins determined by western blot (Fold-change between groups indicated below each band). J) Matched TIL and tumors were derived from the same tumor fragment. The tumor cell line was treated with DMSO or DNA-PKi (2μM NU7441) for 48 hours, at which point drug was washed off prior to co-culture with TIL at a

1:1 ratio for 18 hours. Cytotoxicity as determined by Annexin V staining with flow cytometry gating on tumor cells (based on light scatter and CD3-) and viability dye.

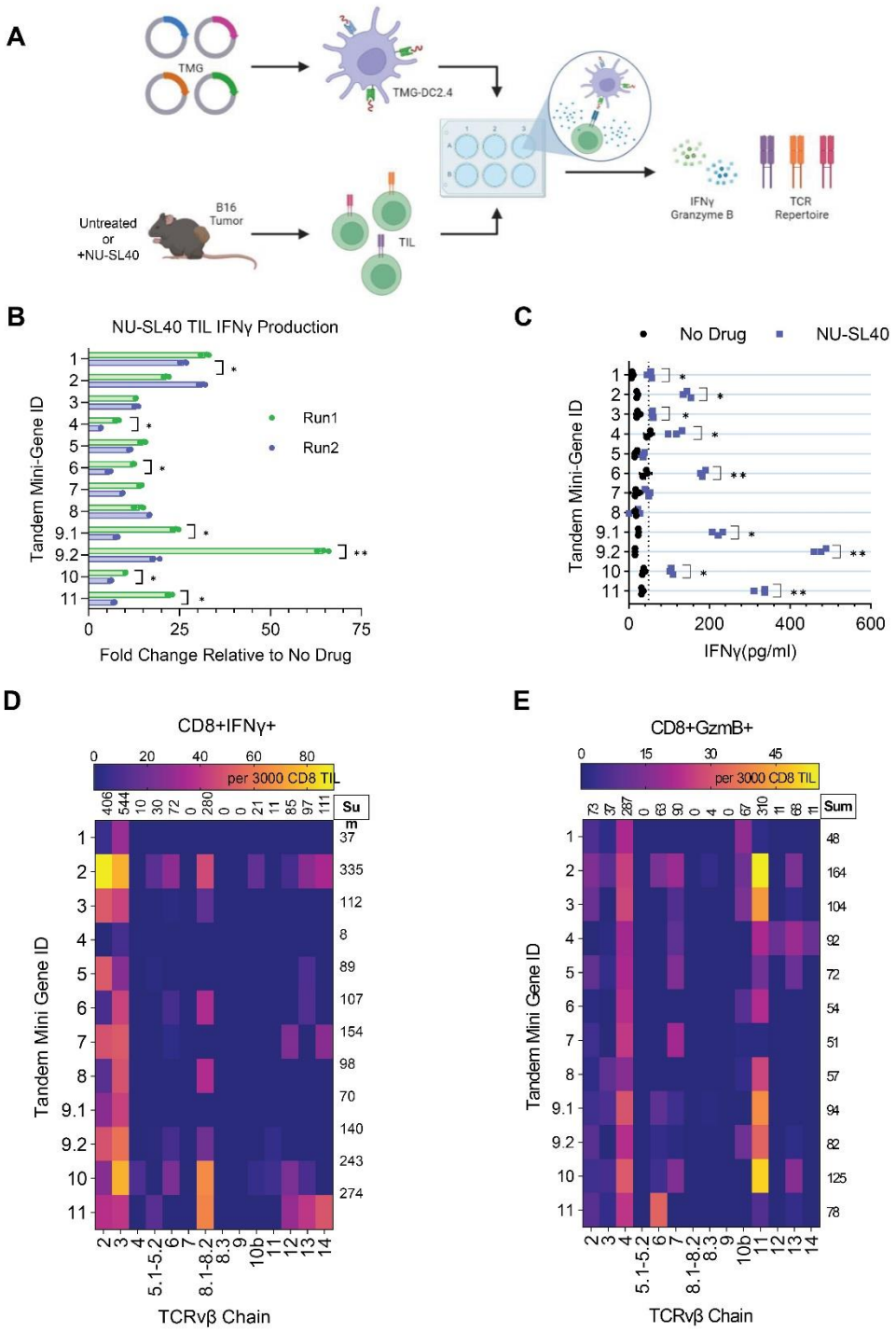


**Figure 5 – DNA-PK inhibitor plus immune adjuvant drives the generation and expansion of a of a unique panel of neoantigen-reactive TILs with enhanced effector function ex vivo.**

**Figure 5 – DNA-PK inhibitor plus immune adjuvant drives the generation and expansion of a unique panel of neoantigen-reactive TILs with enhanced effector function ex vivo.** A) Schematic of experimental design. Mice were treated as described in Figure 3D. TIL were isolated from NU-SL40 or untreated tumors using a positive magnetic selection for CD4 and CD8 T cells. Twelve plasmids were generated to contain tandem minigenes (TMG) of 10 neoantigens identified in Figure 4. B and C) TMGs were transfected into the murine DC2.4 line and co-cultured with CD4 and CD8 TILs collected from control or NUSL40-treated mice (pooled from 10 mice/group) at a 1:10 TIL:DC ratio. After 48 hours IFNγ production by TCRvβ specific responses to DC presented neoantigens was determined by ELISA. Bar graphs depict IFNγ production by TIL stimulated with TMG-DC compared from two independent experiments. Values were normalized to production after stimulation with a TMG-GFP control. D and E) The ability for CD8 TIL to produce IFNγ or GzmB was determined by intracellular staining and flow cytometry. TCRvβ usage in response to stimulation with each TMG-expressing DC was also investigated. Heatmaps represent the number of CD8+ TIL per 3,000 total TIL expressing different TCRvβ chains and producing D) IFNγ or E) GzmB in response to stimulation from each TMG.

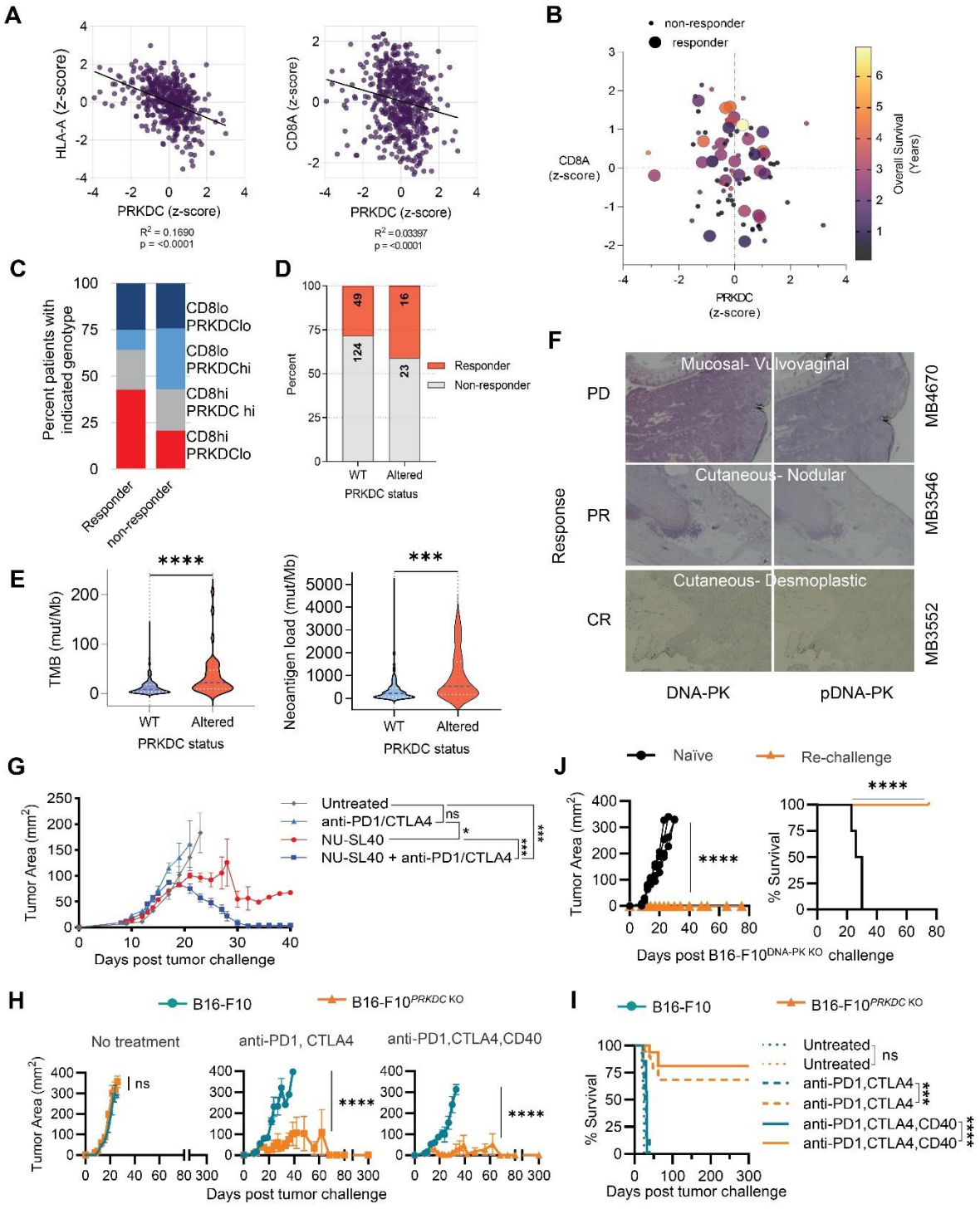


**Figure 6 – *PRKDC* levels inversely correlated with TIL, MHC-I, and response to checkpoint blockade therapy in melanoma patients and is mirrored by B16-F10$^{PRKDC\ KO}$ tumors.**

**Figure 6 – *PRKDC* levels inversely correlated with TIL, MHC-I, and response to checkpoint blockade therapy in melanoma patients and is mirrored by B16-F10$^{PRKDC\ KO}$ tumors.** A) Scatter plot of Z-scores for HLA-A and CD8α expression versus *PRKDC* expression obtained from TCGA. B) Associations between CD8α and *PRKDC* mRNA expression by Z-score with overall survival in months indicated by color scale in responder (large circles) and non-responder (small circles) patients. C) Bar graph distinguishing the percentage of CD8$^{low\ and\ high}$ and PRKDC$^{low\ and\ high}$ between melanoma that responded or not to checkpoint blockade. D) Percentage of melanoma patients expressing wild type (WT) or altered *PRKDC* that responded or not to checkpoint blockade. E) Violin plots depicting differences in Tumor Mutation Burden (left, $p<0.0001$) and Neoantigen Load (right, $p = 0.0002$) in patients with normal (WT, n=172) versus altered (n=40) *PRKDC* expression. Statistical significance was determined by unpaired Mann-Whitney test. F) Staining of melanoma patient samples for total and phosphorylated DNA-PK (Ser2056). G) C57BL/6 mice with established ($25mm^2$) B16-F10 tumors remained untreated or were treated with anti-PD-1/-CTLA-4 blockade, NU-SL40, or NU-SL40 in conjunction with anti-PD-1/-CTLA-4 blockade (n=8/group). Tumor growth was monitored over time. H and I) Wild type B16-F10 (orange) or melanoma cells engineered to knock out *PRKDC* (DNA-PK KO, teal) were injected into mice. When tumors were established, mice were untreated or treated with anti-PD-1/-CTLA-4 with or without anti-CD40 therapy. H) Tumor growth and I) survival were monitored over time (n=8 mice/group). J) Mice treated with combination anti-PD1/-CTLA-4 with anti-CD40 exhibiting tumor control were rechallenged with DNA-PK KO cells after 300 days (naïve; n=4, rechallenge; n=5). Tumor growth and survival were monitored between rechallenged and naïve challenged mice using two-way ANOVA; * $p<0.05$, ** $p<0.01$, *** $p<0.001$, **** $p<0.0001$.